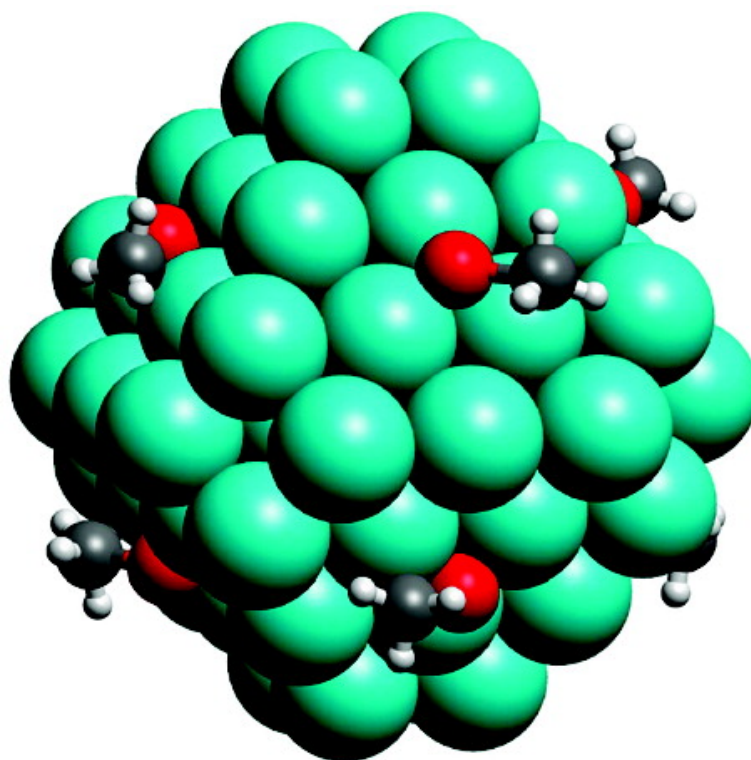Article

How the C#O Bond Breaks during Methanol Decomposition on Nanocrystallites of Palladium Catalysts

Ilya V. Yudanov, Alexei V. Matveev, Konstantin M. Neyman, and Notker Ro#sch

More About This Article

Additional resources and features associated with this article are available within the HTML version:

- Supporting Information
- Links to the 2 articles that cite this article, as of the time of this article download
- Access to high resolution figures
- Links to articles and content related to this article

View the Full Text HTML

How the C−O Bond Breaks during Methanol Decomposition on Nanocrystallites of Palladium Catalysts

Ilya V. Yudanov,[†,‡] Alexei V. Matveev,[†] Konstantin M. Neyman,[§] and
Notker Rösch*,[†]

*Department Chemie, Theoretische Chemie, Technische Universität München, 85747 Garching,
Germany, Boreskov Institute of Catalysis, 630090 Novosibirsk, Russia, and Institució Catalana
de Recerca i Estudis Avançats (ICREA), 08010 Barcelona, IQTCUB & Departament de Química
Física, Universitat de Barcelona, 08028 Barcelona, Spain*

Received October 31, 2007; E-mail: roesch@ch.tum.de

Abstract: Experimental findings imply that edge sites (and other defects) on Pd nanocrystallites exposing mainly (111) facets in supported model catalysts are crucial for catalyst modification via deposition of CH_x ($x = 0-3$) byproducts of methanol decomposition. To explore this problem computationally, we applied our recently developed approach to model realistically metal catalyst particles as moderately large three-dimensional crystallites. We present here the first results of this advanced approach where we comprehensively quantify the reactivity of a metal catalyst in an important chemical process. In particular, to unravel the mechanism of how CH_x species are formed, we carried out density functional calculations of C−O bond scission in methanol and various dehydrogenated intermediates (CH_3O, CH_2OH, CH_2O, CHO, CO), deposited on the cuboctahedron model particle Pd_{79}. We calculated the lowest activation barriers, ~130 kJ mol^{-1}, of C−O bond breaking and the most favorable thermodynamics for the adsorbed species CH_3O and CH_2OH which feature a C−O single bond. In contrast, dissociation of adsorbed CO was characterized as negligibly slow. From the computational result that the decomposition products CH_3 and CH_2 preferentially adsorb at edge sites of nanoparticles, we rationalize experimental data on catalyst poisoning.

1. Introduction

Production of H_2 from methanol is of immediate relevance to practically important problems of methanol-fueled vehicles.[1] On Pd-based catalysts, CH_3OH decomposition occurs with high selectivity toward CO/H_2.[2,3] However, the overall activity is affected by catalyst modification by CH_x ($x = 0-3$) deposits.[4–6] Knowledge on the formation mechanisms of carbonaceous species CH_x on Pd (and other metals) as well as on the nature of intermediates involved is still very limited. Dissociation of CO as source of surface carbon is unlikely even on defect-rich Pd surfaces.[7] Therefore, carbonaceous species CH_x were proposed to arise from the cleavage of C−O bonds, of either
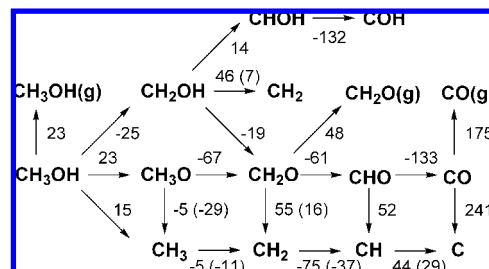

Figure 1. Methanol and selected intermediates of its decomposition: reaction energies (kJ mol^{-1}) for the splitting of C−H, O−H, and C−O bonds as well as for CH_3OH, CH_2O, and CO desorption as calculated on (111) facets of the cluster Pd_{79}. Values in parentheses correspond to CH_x species stabilized at or near cluster edges.

methanol itself or its partially dehydrogenated intermediates CH_xO (Figure 1).[4,8]

C−O bond cleavage has been suggested to occur presumably in those adsorbed intermediates where the C−O bond is tilted, hence activated.[5] According to this proposal, formaldehyde, H_2CO, and formyl, HCO, are the likely candidates for this process, as their C−O bond is oriented almost parallel to the Pd surface in the corresponding adsorption complexes, whereas in adsorbed methoxide, H_3CO, and CO species the C−O axis is oriented essentially perpendicular to the surface.[5] On the other

† Technische Universität München.
‡ Boreskov Institute of Catalysis.
§ ICREA and Universitat de Barcelona.
(1) Holladay, J. D.; Wang, Y.; Jones, E. *Chem. Rev.* **2004**, *104*, 4767.
(2) Usami, Y.; Kagawa, K.; Kawazoe, M.; Matsumura, Y.; Sakurai, H.; Haruta, M. *Appl. Catal., A* **1998**, *171*, 123.
(3) Shiozaki, R.; Hayakawa, T.; Liu, Y. Y.; Ishii, T.; Kumagai, M.; Hamakawa, S.; Suzuki, K.; Itoh, T.; Shishido, T.; Takehira, K. *Catal. Lett.* **1999**, *58*, 131.
(4) Schauermann, S.; Hoffmann, J.; Johánek, V.; Hartmann, J.; Libuda, J.; Freund, H.-J. *Angew. Chem., Int. Ed.* **2002**, *41*, 2532.
(5) Morkel, M.; Kaichev, V. V.; Rupprechter, G.; Freund, H.-J.; Prosvirin, I. P.; Bukhtiyarov, V. I. *J. Phys. Chem. B* **2004**, *108*, 12955.
(6) Borasio, M.; Rodríguez de la Fuente, O.; Rupprechter, G.; Freund, H.-J. *J. Phys. Chem. B* **2005**, *109*, 17791.
(7) Kaichev, V. V.; Morkel, M.; Unterhalt, H.; Prosvirin, I. P.; Bukhtiyarov, V. I.; Rupprechter, G.; Freund, H.-J. *Surf. Sci.* **2004**, *566–568*, 1024.

(8) Rodríguez de la Fuente, O.; Borasio, M.; Galletto, P.; Rupprechter, G.; Freund, H.-J. *Surf. Sci.* **2004**, *566–568*, 740.

hand, a larger π-contribution in the more dehydrogenated intermediates strengthens (stabilizes) the C–O bond. Thus, at least two factors are expected to play a role in the mechanism of C–O bond scission.

Surface morphology and defects also are often discussed as factors that affect C–O bond breaking of methanol on Pd. Recently, it was found that on well-defined supported palladium nanocrystallites exhibiting a high fraction of (111) facets,[9–11] carbon or carbonaceous species CH_x preferentially block defect sites,[4] such as particle edges and steps. These findings may imply an enhanced activity of surface irregularities of nanoparticles in C–O bond cleavage of methanol or intermediates of its dehydrogenation. However, one may invoke an alternative rationalization if CH_x residuals are mobile on the surface and form stronger bonds with sites in the vicinity of edges than at regular sites of interior terrace regions of Pd nanoparticles.

This study is devoted to unraveling the mechanism of C–O bond scission on Pd catalysts as a side process of methanol dehydrogenation reactions, which are notably more rapid. We focus on the role of low-coordinated (edge) sites separating (111) facets of Pd nanocrystallites in accelerating the modification of the catalyst by carbonaceous decomposition products CH_x. A very important methodological aspect of the present work is that we apply here our cluster model approach[12,13] for the first time to quantifying comprehensively the reactivity of a metal catalyst of an important chemical process.

Our modeling scheme deals with nanocrystallites, ∼1 nm in diameter (∼10^2 metal atoms) and terminated by low-index facets only,[12,13] to represent model catalysts which are investigated experimentally.[4–11] Such model catalysts are formed by supported species of few nanometers in diameter (10^3–10^4 metal atoms).[4–11] This cluster model strategy allows one to describe quantitatively adsorption properties of (111) facets of more extended model catalyst particles, but also of the Pd(111) surface.[12] Characteristics of CO adsorption calculated for sites at edges, kinks and (001) terraces of such cluster models afforded an interpretation of peculiarities of the experimental C–O vibrational spectra obtained for defect-rich and well-defined model catalysts.[13] With that strategy, we were also able to quantify bonding and vibrations of CO molecules adsorbed at PdZn[14] nanoclusters and we clarified the location and stability of heteroatom impurities in the subsurface region of Pd nanoparticles.[15] Lately, we studied with these models the adsorption of monatomic carbon species at different sites of Pd nanoparticles.[16]

It was computationally advantageous to carry out these studies[12–16] on models, which exhibit O_h or D_{4h} symmetry. Very recently we were able to reduce the imposed symmetry to group D_4;[17] with this crucial advance, it became feasible to deposit adsorbates *without any local symmetry restrictions* on cluster facets and edges and thus to study complete reaction pathways (including transition states) on both regular and defect sites of sufficiently large metal nanocrystallites.[17]

Invoking this modeling strategy, we address here C–O bond scission of adsorbed intermediates, as it takes place during sequential dehydrogenation of methanol to CO and H_2 on Pd. We calculated the thermodynamics of C–O bond scission as well as the corresponding transition states and activation barriers. We clarified how edges of nanoparticles stabilize in particular C and CH_x species that are formed via this reaction pathway. Dehydrogenation processes are much more facile in the decomposition of methanol than C–O bond scission; the dehydrogenation channel was recently studied in detail for Pd and Pd-based alloys using slab models and a density functional (DF) approach.[18–22] Results of these latter and the present studies provide a database for comparing the two reaction pathways and for elucidating aspects that render the reactivity of regular metal surfaces, such as Pd(111), different from the reactivity of the corresponding nanoparticles.

In the following, we start with computational details and outline salient features of our nanoparticle models. Then, in Section 4 we present our results for adsorption complexes of methanol, pertinent reaction intermediates CH_xO (Sect. 4.1) and CH_x (Sect. 4.2). Subsequently, we discuss reaction energies (Sect. 4.3) and activation barriers (Sect. 4.4) of C–O bond breaking. Finally, in Section 5, we draw conclusions and present an outlook.

2. Computational Details

We carried out all-electron calculations using the linear combination of Gaussian-type orbitals fitting-functions DF (LCGTO-FF-DF) method[23] as implemented in the parallel code PARAGAUSS.[24,25] Self-consistent solutions of the Kohn–Sham equations were obtained with a generalized-gradient approximation (GGA), using the Becke–Perdew (BP) exchange-correlation (xc) functional.[26,27] Because spin-polarized calculations revealed a closed-shell electronic structure of benchmark adsorption complexes, we only discuss results of spin-restricted calculations in the following. To ensure smooth convergence of the electron density during iterations, we applied throughout the technique of fractional occupation numbers with a level broadening of 0.1 eV;[23] we estimate the effect of this approach on the binding energy values to at most 5 kJ mol^{-1}.

(9) Dellwig, T.; Rupprechter, G.; Freund, H.-J. *Phys. Rev. Lett.* **2000**, *85*, 776.

(10) Frank, M.; Bäumer, M. *Phys. Chem. Chem. Phys.* **2000**, *2*, 3723.

(11) Libuda, J.; Meusel, I.; Hoffmann, J.; Hartmann, J.; Piccolo, L.; Henry, C. R.; Freund, H.-J. *J. Chem. Phys.* **2001**, *114*, 4669.

(12) Yudanov, I. V.; Sahnoun, R.; Neyman, K. M.; Rösch, N. *J. Chem. Phys.* **2002**, *117*, 9887.

(13) Yudanov, I. V.; Sahnoun, R.; Neyman, K. M.; Rösch, N.; Hoffmann, J.; Schauermann, S.; Johánek, V.; Unterhalt, H.; Rupprechter, G.; Libuda, J.; Freund, H.-J. *J. Phys. Chem. B* **2003**, *107*, 255.

(14) Neyman, K. M.; Sahnoun, R.; Inntam, C.; Hengrasmee, S.; Rösch, N. *J. Phys. Chem. B* **2004**, *108*, 5424.

(15) Yudanov, I. V.; Neyman, K. M.; Rösch, N. *Phys. Chem. Chem. Phys.* **2004**, *6*, 116.

(16) Neyman, K. M.; Inntam, C.; Gordienko, A. B.; Yudanov, I. V.; Rösch, N. *J. Chem. Phys.* **2005**, *122*, 174705.

(17) Yudanov, I. V.; Neyman, K. M.; Rösch, N. *Phys. Chem. Chem. Phys.* **2006**, *8*, 2396.

(18) Desai, S. K.; Neurock, M.; Kourtakis, K. *J. Phys. Chem. B* **2002**, *106*, 2559.

(19) Schennach, R.; Eichler, A.; Rendulic, K. D. *J. Phys. Chem. B* **2003**, *107*, 2552.

(20) Chen, Z. X.; Neyman, K. M.; Lim, K. H.; Rösch, N. *Langmuir* **2004**, *20*, 8068.

(21) Chen, Z. X.; Lim, K. H.; Neyman, K. M.; Rösch, N. *Phys. Chem. Chem. Phys.* **2004**, *6*, 4499.

(22) Lim, K. H.; Chen, Z. X.; Neyman, K. M.; Rösch, N. *J. Phys. Chem. B* **2006**, *110*, 14890.

(23) Dunlap, B. I.; Rösch, N. *Adv. Quantum Chem.* **1990**, *21*, 317.

(24) Belling, T.; Grauschopf, T.; Krüger, S.; Mayer, M.; Nörtemann, F.; Staufer, M.; Zenger C.; Rösch, N. In *High Performance Scientific and Engineering Computing, Lecture Notes in Computational Science and Engineering*; Bungartz, H.-J., Durst F., Zenger, C., Eds.; Springer: Heidelberg, 1999; Vol. 8, p 439.

(25) Rösch, N. et al. PARAGAUSS, Version 3.1, TU München, Munich, 2004.

(26) Becke, A. D. *Phys. Rev. A* **1988**, *38*, 3098.

(27) (a) Perdew, J. P. *Phys. Rev. B* **1986**, *33*, 8622. (b) Perdew, J. P. *Phys. Rev. B* **1986**, *34*, 7406.

We employed a well-proven orbital basis set for Pd,[12–17] where the original one[28] was extended to (18s,13p,9d) and contracted to [7s,6p,4d] with the help of atomic eigenvectors from scalar relativistic calculations that were carried out with a local density approximation (LDA), namely the VWN xc functional.[29] C and O atoms were described by orbital basis sets (14s,9p,4d), using the original generalized contractions to [6s,5p,2d];[30] the corresponding basis set for H was (8s,4p) → [4s,3p].[30] In the LCGTO-FF-DF method, the Hartree contribution to the electron−electron interaction is evaluated by representing the electron density with the help of an auxiliary basis set[23] that here was constructed in standard fashion by scaling exponents of the orbital basis set.[23] Five p- and five d-type polarization exponents were supplemented (on H p-type only), constructed as geometric series with a factor 2.5, starting with 0.1 au and 0.2 au for p- and d-exponents, respectively. These auxiliary basis sets were of the type (17s,6r^2,5p,5d) for Pd, (14s,9r^2,5p,5d) for C and O, and (8s,4r^2,5p) for H.

Geometry optimizations of adsorbates on the cluster Pd$_{79}$ (see Section 3) were carried out at the nonrelativistic BP GGA level using a relativistic LANL2 effective core potential (ECP) to replace 28 electrons of the 1s-3d core shells of Pd.[31] The basis set for the valence and the outermost core electrons of Pd was contracted as (441/2111/31).[31] The final total energies were obtained in a single-point fashion from all-electron scalar relativistic BP calculations employing a second-order Douglas−Kroll−Hess transformation of the Dirac−Kohn−Sham equation.[32,33] The present combined strategy (single-point all-electron scalar relativistic energies at ECP geometries) is accurate, yet very economic. Binding energies of methoxide, methyl, and oxygen species adsorbed on the cluster Pd$_{79}$ differed at most 5 kJ mol^{-1} from those obtained entirely with an all-electron scalar relativistic approach.[17] Adsorption energies of all species under study were corrected for the basis set superposition error as estimated with the counterpoise technique.[34]

Activation barriers of C−O bond breaking were determined by scanning the potential energy profile along the C−O distance (constrained optimization approach). For each sampling point, the C−O distance was fixed while all other geometry variables of the adsorbed CH$_x$O moiety were optimized. The reaction coordinates in the vicinity of the transition state are estimated to be accurate to 1 pm. The resulting stationary points featured Hessians with one negative eigenvalue, justifying their classification as (approximate) transition states.

3. Nanoparticle Cluster Models

We modeled the substrate with the cuboctahedral cluster Pd$_{79}$, which exposes eight (111) facets and six very small (001) facets (Figure 2a). Adsorbates were deposited symmetrically on each of its (111) facets or edges formed by their intersections. To avoid any local restrictions on position and orientation of adsorbed species on a (111) facet (or edge), we fixed the overall symmetry constraints of the system in agreement with the space group D$_4$ (Figure 2b). This type of models enables adsorbates to cross the cluster edges, which is crucial for studying surface reactions that involve low-coordinated edge sites. Note, that imposing *rotational* symmetry on the models under scrutiny implies that several (here eight) reactions of the same kind take
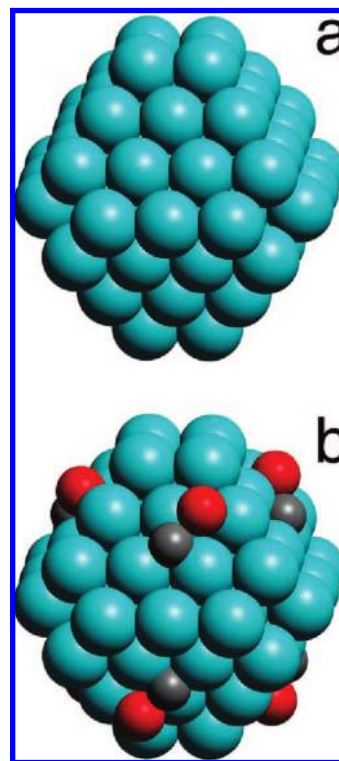

Figure 2. (a) Bare nanocluster Pd$_{79}$ and (b) Pd$_{79}$ with adsorbates deposited at all (111) facets according to D$_4$ symmetry. As an example, the transition state for the dissociation of carbon monoxide is shown.

place simultaneously on equivalent sites of the nanoparticle. This is analogous to the procedure employed with slab models, where *translational* symmetry is exploited instead: there, identical images of a reaction occur within each unit cell. If one models a low-coverage situation, then with either modeling strategy one has to take care to avoid (or sufficiently reduce) interactions between adjacent images.

The structure of the cluster Pd$_{79}$ was kept fixed during all calculations, with Pd−Pd nearest-neighbor distances set to the experimental value of Pd bulk, 275 pm.[35] This strategy reflects two considerations. First, with this nearest-neighbor distance, the cluster Pd$_{79}$ simulates the reactivity of notably larger particles of 300−3000 Pd atoms of experimentally studied model catalysts.[4–11] There, Pd−Pd bond lengths are close to that of bulk Pd, while in a Pd$_{79}$ particle the distances are ∼5 pm shorter.[12,36,37] Thus, cluster relaxation would result in Pd−Pd bonds that are too short to adequately represent the experimental model catalysts; in turn, this would lead to reduced adsorption energies.[12] Second, Pd−Pd distances are considerably overestimated in DF calculations using GGA xc functionals;[37] for instance, slab model calculations with the BP xc functional yield the interatomic distance of Pd bulk at 286 pm.[38] As stated above, such a misrepresentation of the intrasubstrate bonding would affect calculated adsorption properties, especially for transition states of C−O bond scission, because the orientation of the C−O bond on the surface depends on the relative positions of

(28) Huzinaga, S. *J. Chem. Phys.* **1977**, *66*, 4245.
(29) Vosko, S. H.; Wilk, L.; Nusair, M. *Can. J. Phys.* **1980**, *58*, 1200.
(30) Widmark, P.-O.; Malmqvist, P.-A.; Roos, B. O. *Theor. Chim. Acta* **1990**, *77*, 291.
(31) Hay, P. J.; Wadt, W. R. *J. Chem. Phys.* **1985**, *82*, 299.
(32) Häberlen, O. D.; Rösch, N. *Chem. Phys. Lett.* **1992**, *199*, 491.
(33) Rösch, N.; Krüger, S.; Mayer, M.; Nasluzov, V. A. In *Recent Developments and Applications of Modern Density Functional Theory*; Theoretical and Computational Chemistry Series, Vol. 4; Seminario, J. M., Ed.; Elsevier: Amsterdam, 1996; p 497.
(34) Boys, S. F.; Bernardi, F. *Mol. Phys.* **1970**, *19*, 553.

(35) *CRC Handbook of Chemistry and Physics*, 77th ed. Lide, D. R., Ed.; CRC Press: Boca Raton, 1996.
(36) Krüger, S.; Vent, S.; Rösch, N. *Ber. Bunsenges. Phys. Chem.* **1997**, *101*, 1640.
(37) Krüger, S.; Vent, S.; Nörtemann, F.; Staufer, M.; Rösch, N. *J. Chem. Phys.* **2001**, *115*, 2082.
(38) Paul, J.-F.; Sautet, P. *Phys. Rev. B* **1996**, *53*, 8015.

favorable adsorption sites of the reaction products. We also explored an intermediate approach where we fixed the "inner part" Pd_{19} of the cluster Pd_{79} at the bulk geometry and relaxed the outer cluster shell together with adsorbates.[17] At the BP GGA level, we determined only minor relaxation effects, about 3 kJ mol^{-1}, on the calculated adsorption energies of CH_3O and CH_3.[17]

4. Results and Discussion

4.1. Adsorption of Methanol and CH$_x$O Intermediates. The dehydrogenation of methanol on metal surface begins with its adsorption from the gas phase. Adsorbed methanol molecules can desorb, stay intact, or decompose in several steps to produce various CH$_x$O intermediates and surface-bound hydrogen atoms. Besides methanol itself, here we consider the adsorption of the following intermediates on the model cluster Pd_{79} (Figure 3): methoxide (CH_3O), hydroxymethyl (CH_2OH), formaldehyde (CH_2O), formyl (CHO), as well as the final product CO. Most of these intermediates adsorbed on Pd were studied in detail by various theoretical approaches in relation to the main reaction pathway, dehydrogenation.[18–22,39] Thus, in the following we just outline the adsorption modes of these species on Pd clusters and emphasize those characteristics which are important for the mechanism of C–O bond scission.

Methanol. We start by addressing molecular adsorption of methanol on the (111) facets of a Pd_{79} cluster. Electron donation from an oxygen lone pair of methanol to the surface is considered to be an important component of the adsorption interaction on Pd.[40–42] Slab model DF calculations showed that CH_3OH weakly adsorbs on Pd(111) via the O center, with a binding energy of only 30–36 kJ mol^{-1}.[18,42] Our cluster calculations also yield a similarly weak interaction of CH_3OH, calculated at 23 kJ mol^{-1} (Table 1). On a (111) facet of Pd_{79} cluster, a methanol molecule is at a top site (Figure 3a), with a rather long O–Pd bond, 246 pm (Table 2), in line with results of slab model calculations, 225 pm.[42]

Methoxide. Since long ago, alcohol decomposition on Pt-group metals is believed to start with the formation of an alkoxide intermediate via elimination of the hydrogen atom of the hydroxyl group.[40] Stable methoxide intermediates were detected in particular on Pd(111)[43,44] and Pd(100).[45] From results of DF calculations on Pt(111)[18,46] and Pd(111),[18] the formation of hydroxymethyl CH_2OH via elimination of a H atom from the C center (of methanol) was suggested to be competitive. Yet, there is still little experimental evidence for the latter route on Pd, where according to DF results[18,46] the formation of CH_2OH is less favorable than on Pt. Thus, the present study focuses on the methanol dehydrogenation route through methoxide, formaldehyde, and formyl to carbon monoxide, *all intermediates* of which were *experimentally detected* on Pd catalysts in the course of methanol decomposition.[6,43]

DF cluster[39,47] and slab model[18,20] calculations showed that hollow sites are favored for methoxide adsorption on Pd(111).
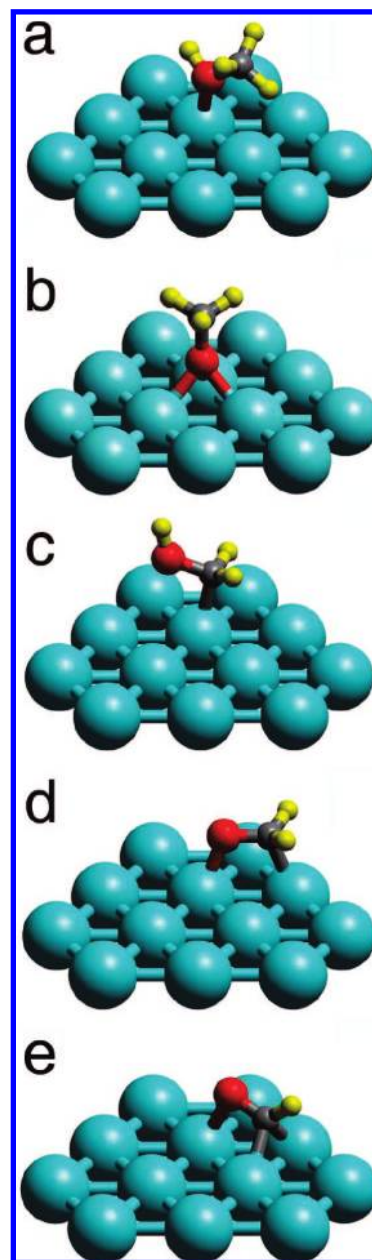

Figure 3. Adsorption complexes on a (111) facet of the nanocrystallite Pd_{79}: (a) methanol CH_3OH, (b) methoxide CH_3O, (c) hydroxymethyl CH_2OH, (d) formaldehyde CH_2O, and (e) formyl CHO. The (111) facet shown is oriented as the front facet of the Pd_{79} cluster in Figure 2.

Slab model calculations with the GGA-PW91 *xc* functional[48] yielded binding energies of 162 and 153 kJ mol^{-1} for methoxide adsorption at fcc and hcp hollow sites of Pd(111), respectively.[20] The (111) facets of the cluster model Pd_{79}, adopted in present study, feature an fcc site at their center. Methoxide (actually, each of eight molecules) was calculated to bind at this position of the cluster Pd_{79} (Figure 3b) with an adsorption energy of 160 kJ mol^{-1} (Table 1). Such good agreement between cluster and slab model calculations is not surprising. Indeed, we demonstrated for the example of CO (using consistent *xc* functionals) that adsorption at the central positions of (111) facets of nanocluster models already of this size affords an accurate representation of adsorption complexes at an infinite

(39) Neurock, M. *Top. Catal.* **1999**, *9*, 135.
(40) Bowker, M.; Madix, R. J. *Surf. Sci.* **1980**, *95*, 190.
(41) Mavrikakis, M.; Barteau, M. A. *J. Mol. Catal. A* **1998**, *131*, 135.
(42) Zhang, C. J.; Hu, P. *J. Chem. Phys.* **2001**, *115*, 7182.
(43) Davis, J. L.; Barteau, M. A. *Surf. Sci.* **1987**, *187*, 387.
(44) Guo, X.; Yates, J. T. *J. Am. Chem. Soc.* **1989**, *111*, 3155.
(45) Christmann, K.; Demuth, J. E. *J. Chem. Phys.* **1982**, *76*, 6308.
(46) Greeley, J.; Mavrikakis, M. *J. Am. Chem. Soc.* **2004**, *126*, 3910.
(47) Kua, J.; Goddard III, G. A. *J. Am. Chem. Soc.* **1999**, *121*, 10928.

(48) Perdew, J. P.; Wang, Y. *Phys. Rev. B* **1992**, *45*, 13244.

Table 1. Calculated Desorption Energies $\Delta E_{des} \equiv -\Delta E_{ads}$, Energies ΔE_{C-O} of C–O Bond Scission,[a] Activation Barriers $\Delta E^{\#}_{C-O}$ of C–O Bond Scission, and Reaction Energy ΔE_{X-H} of C–H (O–H) Bond Scission Calculated for Methanol and Its Intermediates on the Nanocrystallite Pd_{79} (in kJ mol^{-1})

	ΔE_{des}	$\Delta E_{C-O}{}^{a}$	$\Delta E^{\#}_{C-O}$	ΔE_{C-H}	ΔE_{O-H}
CH_3OH	23	15	158	−25	23
CH_3O	160	−5 (−29)	135	−67	−
CH_2OH	156	46 (7)	128	14	−19
CH_2O	48	55 (16)	194	−61	−
CHO	230	52	206	−133	−
CO	175	241	414	−	−

[a] Values taking into account the stabilization of CH_2 and CH_3 products at cluster edges between the (111) facets are given in parentheses.

Table 2. Selected Interatomic Distances (in pm) Calculated for Methanol and the Intermediates of Its Decomposition in the Gas Phase (g.p.), Adsorbed on (111) Facets of the Nanocrystallite Pd_{79} (ads.) and in the Corresponding Transition States (TS) of C–O Bond Scission

	g.p.	ads.			TS		
	C–O	C–O	C–Pd	O–Pd	C–O	C–Pd	O–Pd
CH_3OH	143	143	−	246	194	240	219
CH_3O	136	143	−	224	189	219	202
							203
							205
CH_2OH	137	141	209	273	251	188	204
CH_2O	121	132	212	209	249	189	198
							199
CHO	119	126	200	224	194	192	205
			211			196	209
						212	
CO	114	119	204	−	200	187	205
						194	210
						201	

(111) surface.[12] We calculated the C–O bond of adsorbed methoxide at 143 pm (Table 2), just as that of the free methanol molecule, but 7 pm longer than that of the methoxide radical in the gas phase. The unpaired electron of the latter molecule occupies a π orbital, which features a strong oxygen contribution. The elongation of the C–O bond in adsorbed methoxide reflects the fact that this π contribution to the C–O bond is essentially eliminated when O $2p$ orbitals orthogonal to the C–O axis form bonds to the Pd centers of the 3-fold hollow adsorption site.

Hydroxymethyl. As various pathways of methanol decomposition on Pt(111) were recently discussed on the basis of DF calculations,[46] we consider here also hydroxymethyl, CH_2OH, as alternative intermediate. This species forms by hydrogen abstraction from the carbon center of methanol instead of the oxygen center. According to slab model DF calculations, formation of CH_2OH is favored over formation of CH_3O by about 80 kJ mol^{-1} on Pt(111) and by 40 kJ mol^{-1} on Pd(111).[18] Also the corresponding activation barrier on Pt(111), 92 kJ mol^{-1}, was calculated lower than the barrier, 142 kJ mol^{-1}, for the formation of CH_3O.[18] On both Pt(111) and Pd(111), CH_2OH prefers on-top adsorption through the carbon atom.[18] We calculated the formation of CH_2OH from CH_3OH on (111) facets of Pd_{79} (Figure 3c) to be exothermic, $\Delta E = -48$ kJ mol^{-1}, while formation of the CH_3O intermediate is thermoneutral, 0.3 kJ mol^{-1} (Figure 1). The calculated desorption energy of CH_2OH on Pd_{79} is 156 kJ mol^{-1}, only marginally smaller than that of CH_3O (Table 1). Slab model calculations yielded 179 kJ mol^{-1} for CH_2OH and 171 kJ mol^{-1} for CH_3O.[18] The somewhat higher energies of the slab model calculations

may be associated with the use of the PW91 xc functional, which is known to yield often larger metal–ligand binding energies than the BP functional employed here.[49,50]

Mechanistic details of the initial step of methanol dehydrogenation on Pd are beyond the scope of the present work. Yet, one can refer to experience collected for Pt analogues, where preadsorbed oxygen likely promotes the dissociation of the OH group of CH_3OH, producing the CH_3O intermediate.[51,52] Surface oxygen centers can act as Brønsted base sites which facilitate the removal of hydrogen from the OH group because the latter is more acidic than hydrogen of methyl moieties.[18] DF slab model calculations have been performed on the competitive dehydrogenation of CH_2OH on Pt(111) to hydroxymethylene, CHOH, and to formaldehyde, CH_2O.[46] Accordingly, among these intermediates CHOH is favored over CH_2O, both thermodynamically (by 43 kJ mol^{-1}) and kinetically (by 12 kJ mol^{-1}), but the reaction remains slightly endothermic on Pt(111). At variance, on a Pd_{79} particle our calculations favor by 33 kJ mol^{-1} (Figure 1, Table 1) the dehydrogenation of CH_2OH to CH_2O over the path to CHOH, which adsorbs asymmetrically at a bridge site of a (111) facet. Our calculations predict the decomposition of adsorbed CHOH to CHO or COH to be strongly exothermic. These data indicate that Pt and Pd catalysts exhibit diverse reactivity in various C–H bond-breaking steps of methanol decomposition.

As we will focus in the following on the activation of the C–O bond, note that the C–O distance of adsorbed CH_2OH, 141 pm (Table 2), is 4 pm elongated compared to the free molecule CH_2OH, and 2 pm shorter than in adsorbed CH_3O and the free molecule CH_3OH. The C–O distance is calculated to shorten further for adsorbed CHOH (136 pm) and COH (133 pm). Thus, in line with results discussed below (Tables 1 and 2; Sect. 4.4), these two intermediates on Pd appear to be less prone to C–O bond scission than CH_2OH, CH_3O and CH_3OH, where the bond is longer (weaker).

Formaldehyde. CH_2O molecules adsorb on transition metals in two bonding modes, η^1-(O) and η^2-(C,O).[40] In the η^1-(O) configuration, the molecule binds to the surface via the O center using one of its lone pairs.[40] In the η^2-(C,O) mode (Figure 3d), the adsorbate interacts with the substrate via both centers, C and O. This adsorption mode is generally preferred on clean surfaces of group VIII metals.[40] In contrast, surfaces precovered by oxygen promote the η^1-(O) configuration of aldehydes, in which they tend to desorb rather than to decompose further. Indeed, η^1-(O) configurations of formaldehyde were found to be unstable on the clean Pd(111) surface in DF slab model calculations.[20]

The η^2-(C,O) adsorption complex exhibits a top-bridge-top structure with the CO group of CH_2O almost parallel to the surface, such that the Pd–C and Pd–O bonds are almost equal in length.[18,20,22] Our calculations yielded essentially the same structure of the η^2-(C,O) adsorption complex (Pd–C = 212 pm, Pd–O = 209 pm; Table 2, Figure 3d) as slab model calculations for the extended Pd(111) surface.[20,22] The calculated binding energy, 48 kJ mol^{-1} (Table 1), is close to the value of 50 kJ

(49) Matveev, A.; Staufer, M.; Mayer, M.; Rösch, N. *Int. J. Quantum Chem.* **1999**, *75*, 863.
(50) Görling, A.; Trickey, S. B.; Gisdakis, P.; Rösch, N. In *Topics in Organometallic Chemistry*; Brown J., Hofmann, P., Eds.; Springer: Heidelberg, 1999; Vol. 4, p 109.
(51) Akhter, S.; White, J. M. *Surf. Sci.* **1986**, *167*, 101.
(52) Endo, M.; Matsumoto, T.; Kubota, J.; Domen, K.; Hirose, C. *Surf. Sci.* **1999**, *441*, L931.

mol^{-1} determined from temperature-programmed-desorption data[53] as well as to results of slab model calculations, 43−61 kJ mol^{-1}.[18–20,22] Thus, formaldehyde forms the weakest bond with the surface among all intermediates of the methanol dehydrogenation pathway (Table 1); only methanol itself interacts more weakly (see above). Despite this weak interaction, the C−O bond of adsorbed CH_2O is substantially elongated, 9 pm, compared to the free molecule, where the C−O distance was calculated at 121 pm (Table 2). C−H bonds of adsorbed CH_2O point away from the surface. The angles at the carbon center, $\angle OCH = 116°$ and $\angle PdCH = 98°$, imply a propensity to rehybridization from sp^2 to sp^3, that weakens (and elongates) the C−O bond with respect to a free CH_2O molecule.

Formyl. According to DF slab model calculations, CHO does not exhibit a clear preference for specific adsorption site of Pd(111): adsorption energies of various sites differ less than 15 kJ mol^{-1}.[22] No wonder that different adsorption sites were reported to be most stable: the η^1-(C) configuration,[22] where carbon binds on-top (C−Pd = 199 pm) with $\Delta E_{ad} = -214$ kJ mol^{-1},[22] and the η^2-η^1(C,O) configuration[18] with carbon located over a Pd−Pd bridge and the O atom on-top of an adjacent Pd atom, $\Delta E_{ad} = -237$ kJ mol^{-1}. As both studies employed the same xc functional PW91, the large difference (23 kJ mol^{-1}) between these two adsorption energies likely is due to the different quality of the substrate models: the slabs consisted of four[22] or three[18] layers of metal atoms, respectively. With the nanocluster model of the present work, CHO species were calculated to adsorb in an η^2-η^1-(C,O) configuration (Figure 3e, Table 2). The C−Pd distances to two atoms of the Pd−Pd bridge are 200 and 211 pm, while the distance O−Pd to the third Pd center is considerably longer, 224 pm (Table 2). The C−O bond elongates from 119 pm in free CHO to 126 pm in the adsorption complex. Similarly to adsorbed formaldehyde, this elongation can be rationalized by partial rehybridization of the C center, which is sp^2-hybridized in the gas-phase species ($\angle OCH = 124°$), but exhibits a sp^3 configuration upon interaction with the substrate, as manifested by bond angles in adsorbed formyl, $\angle OCH = 118°$ and $\angle OCPd = 113°$ (2×). The calculated energy of formyl desorption from Pd$_{79}$, 230 kJ mol^{-1}, agrees well with slab model results, 237 or 214 kJ mol^{-1},[18,22] from calculations on slabs with different numbers of metal layers.

At variance with other intermediates of methanol decomposition, adsorption complexes of formyl on Pd(111) appeared as problematic cases in an earlier cluster model study,[39] because adsorption energies showed large deviations from slab model results. The energy of desorption of CHO from a two-layer cluster Pd$_{19}$ was calculated at 340 kJ mol^{-1} (BP86),[39] that is, ∼100 kJ mol^{-1} more than with a three-layer slab of Pd(111) (PW91),[18] while for other intermediates (CH$_3$O, CH$_2$O, etc.) the difference between cluster and slab model results did not exceed 20 kJ mol^{-1}.[18]

As our calculations with the model cluster Pd$_{79}$ were carried out using the same xc functional BP86 as in that earlier study on the Pd$_{19}$ model[39] and produced adsorption energy in the same range as various slab model calculations,[18,22] the notable overestimation of the CHO adsorption energy calculated with Pd$_{19}$ seems to be due to an inadequate representation of metal substrate in that model. Although the top layer of that substrate cluster model[39] was of the same size and shape as the cluster facets of the present Pd$_{79}$ model (12 atoms, Figure 2), the layer underneath of only 7 atoms was obviously too small to
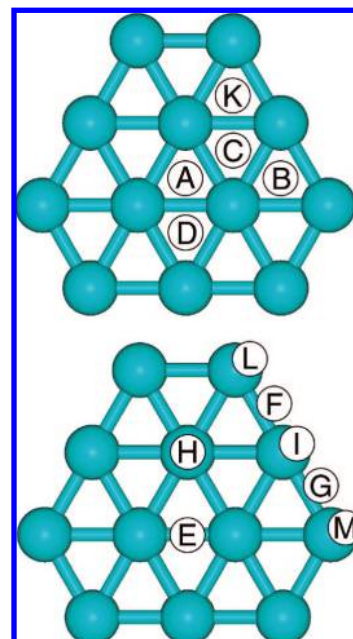
(53) Davis, J. L.; Barteau, M. A. *J. Am. Chem. Soc.* **1989**, *111*, 1782.

Figure 4. Adsorption sites at a (111) facet of Pd$_{79}$ (A, B, E, H, K) and at edges (F, G, I, L, M) of this particle: 3-fold hollow μ_3 A, B, K (fcc) and C, D (hcp); bridge μ_2 E, F, and G; on-top μ_1 H, I, L, M.

reproduce the properties of an extended metal substrate. Moreover, most centers of that two-layer Pd$_{19}$ model are located at cluster boundaries and, therefore, the fraction of metal atoms exhibiting low coordination, hence unsaturated bonds, seems too large to afford results that are sufficiently representative for an extended substrate.[12] This case nicely illustrates the adequacy and internal consistency of our model approach, which describes adsorbate−substrate interactions with the help of moderately large (three-dimensional) nanocrystallites, terminated *exclusively* by low-index planes. All metal centers of the two-layer Pd$_{19}$ model[39] were treated as nonequivalent by symmetry to allow for an arbitrary orientation of adsorbates on the surface. The three-dimensional cluster Pd$_{79}$ of the present study exhibits the same quality for modeling the deposition of adsorbates; in fact, the quality is even better as edges of Pd$_{79}$ represent physically meaningful sites in contrast to the edges of the two-layer cluster Pd$_{19}$. This higher quality of our Pd$_{79}$ model is achieved with comparable computational expenditure, as D$_4$ symmetry constraints leave only 13 nonequivalent Pd centers to be treated in Pd$_{79}$.

Carbon Monoxide. The most stable adsorption on Pd nanocrystallites was calculated at bridge sites of cluster edges (Pd$_{146}$).[13] On (111) facets of Pd nanocrystallites (Pd$_{79}$ to Pd$_{146}$), CO occupies 3-fold hollow sites with very similar energies for fcc or hcp sites.[12,13] Here, we calculated a CO binding energy of 175 kJ mol^{-1} at the central fcc site of the (111) facet of the Pd$_{79}$ model. We discussed CO adsorption on Pd nanoclusters in detail elsewhere; there, we also assessed the effect of the xc approximation by comparison with experimental adsorption energies.[12,13]

Oxygen, Hydrogen, and OH. As reference for quantifying energies of C−O and C−H bond scission in different intermediates adsorbed on a Pd$_{79}$ model cluster, we used O, H, and OH species adsorbed on the (111) facets of Pd$_{79}$ (Figure 4). We determined preferred adsorption sites and calculated the following desorption energies: 430 kJ mol^{-1} for O at a 3-fold hollow site (μ_3[A], here the lower index corresponds to the number

Table 3. Desorption Energies $\Delta E_{des} \equiv -\Delta E_{ads}$ (in kJ mol^{-1}) of CH$_x$ Species at Different Sites of the Nanocrystallite Pd$_{79}$

site[a]	CH$_3$	CH$_2$	CH	C
$\mu_3{}^A$	117	374	639	645
$\mu_3{}^B$			628	651
$\mu_3{}^C$			622	639
$\mu_3{}^D$				604
$\mu_2{}^E$	131	383	554	567
$\mu_2{}^F$		402		
$\mu_2{}^G$		410		
$\mu_1{}^H$	159		345	392
$\mu_1{}^I$	182			
$\mu_1{}^L$	172			
$\mu_1{}^M$	177			

[a] For the designation of the adsorption sites, see the text and Figure 4.

of Pd centers forming the adsorption site, while the upper index refers to the position on (111) facets of a Pd$_{79}$ cluster as shown in Figure 4); 325 kJ mol^{-1} for H at $\mu_3{}^A$; 229 kJ mol^{-1} for OH on top of a Pd center ($\mu_1{}^H$).

Summarizing some trends, we note that the orbital structure of adsorbed intermediates of methanol dehydrogenation features increasing π-character of the C−O bonds with increasing degree of dehydrogenation: a pure σ bond in CH$_3$OH as well as adsorbed CH$_3$O and CH$_2$OH, one occupied π orbital in adsorbed CH$_2$O and CHO and (formally) two occupied π orbitals in adsorbed CO. Concomitantly, the C−O interaction becomes stronger along this series of intermediates, as monitored by the contraction of the C−O bond. At the beginning of dehydrogenation, the intermediate CH$_3$O is coordinated to the Pd surface by its O atom, Figure 3b (or by the C center in the case of the alternative pathway involving hydroxymethyl, Figure 3c). After the next dehydrogenation step, the C−O axis of CH$_2$O is almost parallel to the surface, Figure 3d; CHO also binds by both O and C atoms, Figure 3e, although the C-surface distance is shorter. Finally, CO is bound to the surface via the C center.

4.2. Adsorption of CH$_x$ Species. Next we consider adsorption of CH$_x$ species ($x = 0$−3) as products of C−O bond breaking in CH$_x$O intermediates of methanol dehydrogenation on Pd catalysts. In view of experimental indications that CH$_x$ fragments tend to preferentially occupy adsorption sites at or near the edges of nanoparticles,[5] we paid particular attention to CH$_x$ adsorption at such edge positions.

Methyl. We begin with adsorption in the immediate vicinity of the center of (111) facets. In agreement with slab-model results,[20] CH$_3$ exhibits the strongest binding on a facet in an on-top configuration, 159 kJ mol^{-1} ($\mu_1{}^H$, Figure 4). In this adsorption complex, the C_3 axis of CH$_3$ is perpendicular to the (111) plane. The binding energies for bridge ($\mu_2{}^E$, Figure 4) and fcc hollow sites are smaller, 131 and 117 kJ mol^{-1}, respectively (Table 3). GGA-PW91 slab model calculations yielded 170 and 152 kJ mol^{-1} for on-top and fcc sites of Pd(111), respectively.[20] Thus, the potential energy surface of the present cluster model is more corrugated regarding the adsorption positions of CH$_3$ on (111) facets than that calculated for the slab model of the infinite (111) surface. However, CH$_3$ forms the strongest bond on the Pd$_{79}$ nanocluster, 182 kJ mol^{-1}, on top of a Pd atom located in the middle of the cluster edge ($\mu_1{}^I$, Figure 4). Adsorption on-top of corner Pd centers, where a (001) facet intersects with two (111) facets is slightly weaker, 172 kJ mol^{-1} for $\mu_1{}^L$ and 177 kJ mol^{-1} for $\mu_1{}^M$ (Figure 4, Table 3). Repulsion between symmetrically coadsorbed species is presumably responsible for weakening the adsorption interaction at the latter corner positions compared to the edge position $\mu_1{}^I$.

Indeed, the weaker adsorbed methyl moiety at a $\mu_1{}^L$ edge site interacts with three nearby CH$_3$ groups deposited, according to the symmetry-induced 4-fold replication, while the stronger adsorbed species at $\mu_1{}^M$ interacts with a single symmetry-induced congener (C_2 rotation).

Methylene. In agreement with slab model results,[54] CH$_2$ species on a (111) facet of the Pd cluster preferentially adsorb at bridge sites with a binding energy of 383 kJ mol^{-1} and an almost tetrahedral coordination of the carbon center: ∠HCH = 111°, ∠PdCH = 112° ($\mu_2{}^E$, Figure 4, Table 3). Slab model calculations on the Pd(111) surface furnished somewhat smaller energies, 353 kJ mol^{-1} (PW91) and 345 kJ mol^{-1} (BP).[38] CH$_2$ likely is highly mobile on a Pd(111) facet or surface; the diffusion barrier can be estimated from the binding energy of CH$_2$ at the hollow fcc site ($\mu_3{}^A$, Figure 4) that is only by 9 kJ mol^{-1} smaller than at the neighboring bridge site. Slab model calculations also yielded a rather small energy difference between bridge and hollow sites, 18 kJ mol^{-1}.[38] Similarly to CH$_3$, CH$_2$ species are stabilized at cluster edges (Figure 4, Table 3); the binding energies of the two bridge adsorption sites considered at the cluster edge are 402 kJ mol^{-1} ($\mu_2{}^F$) and 410 kJ mol^{-1} ($\mu_2{}^G$).

C and CH. Both C and CH prefer adsorption at 3-fold hollow sites with similar adsorption energies. Thus, in agreement with findings for the Pd(111) surface[38] and other platinum-group metals,[55–58] adsorbed hydrocarbon CH$_x$ fragments tend to approach the tetravalent state of carbon. On Pd$_{79}$, CH$_3$ is preferably adsorbed on-top, CH$_2$ favors a bridge (2-fold) site, and adsorption of CH as well as C is most stable at 3-fold hollow sites. [Note that a carbon atom interacts even more strongly with the four Pd atoms of the very small Pd(100) facets of Pd$_{79}$.[16]] We calculated binding energies of 645 kJ mol^{-1} for C and 639 kJ mol^{-1} for CH at the central fcc site $\mu_3{}^A$ (Figure 4) of the (111) facet of the cluster Pd$_{79}$. The C−H axis of the CH adsorption complex is perpendicular to the (111) facet. The binding energy of a carbon species agrees with the results of our previous study,[16] where we calculated 639 kJ mol^{-1} (Pd$_{79}$) and 635 kJ mol^{-1} (Pd$_{85}$) for adsorption at central fcc sites of (111) facets and 636 kJ mol^{-1} (Pd$_{140}$) to 632 kJ mol^{-1} (Pd$_{146}$) for adsorption at central hcp sites of (111) facets of larger clusters.[16] Slab model calculations (BP86) on Pd(111) resulted in binding energies of 618 kJ mol^{-1} (C) and 569 kJ mol^{-1} (CH),[38] thus showed a more pronounced difference between C and CH than our cluster calculations.

Comparison to that slab model study of CH$_x$ species[38] reveals notably higher differences to our cluster model results for species adsorbed in central positions of (111) facets than so far observed for other adsorbates, starting from CO adsorption[12,13] up to the present study of CH$_x$O intermediates (see previous subsection). One reason for these discrepancies likely is the slab thickness of only two layers (or three layers for single-point energy calculations) used in that work.[38] Furthermore, those models[38] with 1/3 ML coverage appear to be associated with non-negligible intra-adsorbate repulsion.[59] For comparison, PW91

(54) Paul, J.-F.; Sautet, P. *J. Phys. Chem. B* **1998**, *102*, 1578.
(55) Minot, C.; van Hove, M. A.; Somorjai, G. A. *Surf. Sci.* **1982**, *127*, 441.
(56) Zheng, C.; Apeloig, Y.; Hoffmann, R. *J. Am. Chem. Soc.* **1988**, *110*, 749.
(57) van Santen, R. A.; de Koster, A.; Koerts, T. *Catal. Lett.* **1990**, *7*, 1.
(58) Abild-Pedersen, F.; Greeley, J.; Studt, F.; Rossmeisl, J.; Munter, T. R.; Moses, P. G.; Skulason, E.; Bligaard, T.; Nørskov, J. K. *Phys. Rev. Lett.* **2007**, *99*, 016105.
(59) Lim, K. H.; Neyman Rösch, K. M. *Chem. Phys. Lett.* **2006**, *432*, 184.

binding energies of atomic C on a four-layer slab at 1/9 coverage, calculated in single-point fashion, exhibited similar trends as the present nanocluster models: 641 kJ mol^{-1} at fcc sites (Pd−C =185.5 pm) and 648 kJ mol^{-1} at hcp sites;[16] the corresponding values at coverage 1/4 were ∼20 kJ mol^{-1} smaller.

At other sites of the (111) facet carbon atoms adsorb weaker than at the central hollow site. Adsorption energies differ by 253 kJ mol^{-1} for the on-top position (μ_1^H) and by 78 kJ mol^{-1} for the bridge position (μ_2^E) (Figure 4, Table 3). Apparently, the C center of the adsorbate exhibits a clear propensity to achieving a tetrahedral bonding configuration; the resulting enhanced stability is associated with a reduced mobility of the adsorbate on the surface. Also, in our previous study on the cluster Pd$_{140}$,[13] the bridge position at the cluster edge was calculated ∼50 kJ mol^{-1} less stable than the favored hollow site of the (111) facet. For CH, on-top μ_1^H and bridge μ_2^E adsorption on the (111) facet (Figure 4) is 294 and 85 kJ mol^{-1}, respectively, less stable than adsorption at the hollow site μ_3^A (Table 3).

It is instructive to examine how the stability of C and CH species at different hollow sites of a (111) facet varies with the distance from the edges. In a previous study, we noted a significant destabilization of carbon species near cluster edges.[16] However, in that study,[16] O$_h$ and D$_{4h}$ symmetry constraints did not permit us to consider isolated carbon species in the vicinity of a cluster edge. Rather, when a carbon atom was deposited at a hollow site close to a cluster edge, there was a symmetry-equivalent carbon atom located in the vicinity, at the adjacent (111) facet of the same edge. Thus, it was not possible to distinguish between two effects: (i) the repulsion between two (partially negatively charged) carbon species and (ii) the influence of the edge on the adsorption energy. Presently, with symmetry reduced to D$_4$, we found only minor variations of the adsorption energy of isolated C and CH species located near a cluster edge, compared to the adsorption complexes at the center of (111) facets. Indeed, we calculated binding energies of 651 and 643 kJ mol^{-1} for carbon at μ_3^B fcc and μ_3^C hcp positions, respectively, near an edge (Figure 4, Table 3). For CH at the same sites we obtained 628 and 622 kJ mol^{-1}, respectively. Thus, for C species these energy deviations of ± 6 kJ mol^{-1} compared to the central μ_3^A fcc site are negligible, while for CH one may diagnose a rather weak trend to weaker adsorption interactions (by 10−15 kJ mol^{-1}) at hollow positions near an edge that separates two neighboring (111) cluster facets. More important, however, is the repulsion between two adsorbed carbon species that are approaching the same edge of adjacent (111) facets. We can illustrate this by comparing μ_3^D and μ_3^C hcp sites (Figure 4), which are equivalent by cluster topology but represent differ situations of adsorbate coverage: μ_3^C complexes, calculated in D$_4$ symmetry, represent isolated C adsorbates (see above), whereas μ_3^D complexes imply two C atoms to be on different (111) facets near the same edge. At μ_3^D sites, the binding energy of C was calculated 35 kJ mol^{-1} smaller than at μ_3^C sites. On the basis of this result, the destabilization of adsorbed C species near cluster edges in a high-coverage situation[16] should be assigned to lateral repulsion between nearby carbidic C$^{-\delta}$ species.

Summarizing these calculated adsorption data for CH$_x$ species on a Pd$_{79}$ particle, we can highlight the following general trends: (i) configurations of adsorption complexes agree with the propensity of CH$_x$ adsorbates to exhibit sp^3 hybridization at the carbon center (on top adsorption for CH$_3$, bridge for CH$_2$, 3-fold

for C and CH) which is quite natural for carbonaceous species forming an adsorption complex on a metal surface with a closed-shell electronic structure;[55–57] (ii) the binding energies per Pd−C bond increase from 160−180 kJ mol^{-1} for CH$_3$ to 190−200 for CH$_2$ and ∼210 kJ mol^{-1} for C and CH; (iii) CH$_3$ and CH$_2$ species prefer adsorption complexes on cluster edges over those on (111) facets; (iv) CH$_3$ and CH$_2$ are more mobile on the surface than C and CH moieties, if one takes the variation of adsorption energies as indicator for a smaller corrugation of the potential energy surface of CH$_3$ and CH$_2$ species. For instance, the energy profile for CH$_3$ diffusion along the path top-bridge-top on a (111) facet is characterized by an activation barrier of ∼30 kJ mol^{-1}, as estimated by comparing adsorption energies on corresponding positions (Table 3), while we estimated barriers for the diffusion of C and CH along the path μ_3-bridge-μ_3 at ∼80 kJ mol^{-1}.

4.3. Reaction Energies of C−O Bond Scission in CH$_3$OH and CH$_x$O Intermediates. The reaction energies of C−O bond scission in CH$_x$O intermediates were calculated with respect to adsorption complexes of intermediates and products at the most stable sites of the (111) facet of a Pd$_{79}$ cluster as discussed above. We did not account for the interaction of coadsorbed products, i.e., reaction energies were estimated from energies of separate adsorption complexes of CH$_x$ and O on a Pd$_{79}$ cluster (or OH in the case of CH$_3$OH and CH$_2$OH decomposition). Table 1 collects the reaction energies, ΔE_{C-O}, of C−O bond scission, calculated in this way; for comparison, we also list desorption energies, $-\Delta E_{ads}$. As we had identified a trend for stabilization of CH$_2$ and CH$_3$ species at cluster edges in the preceding subsection, the reaction energies corrected for this effect are also given (in parentheses, Table 1) for the intermediates CH$_2$O, CH$_3$O, and CH$_2$OH, which produce CH$_2$ and CH$_3$ by scission of the C−O bond. In those cases, the energies of CH$_2$ and CH$_3$ adsorbed at the most stable edge positions (bridge or on-top, respectively) were taken as reference, whereas O (and OH) species are still considered in their most stable positions on the (111) facets.

The data presented in Table 1 show that on regular (111) facets of a Pd nanoparticle C−O bond scission is slightly exothermic (or almost thermoneutral) only in the case of methoxide species. The reaction energy of −5 kJ mol^{-1} for C−O bond scission in CH$_3$O on (111) facets of Pd$_{79}$ is very close to the reaction energy on the extended Pd(111) surface, 5 kJ mol^{-1}, according to slab model results.[22] C−O bond scission in hydroxymethyl, formaldehyde, and formyl is moderately endothermic, by ∼50 kJ mol^{-1}. For CH$_2$O (similar to CH$_3$OH), the C−O bond scission energy was calculated to be of almost the same size as the desorption energy. Dissociation of CO was calculated to be thermodynamically the most unfavorable C−O bond breaking: this reaction is endothermic by 241 kJ mol^{-1} whereas ∼60 kJ mol^{-1} less are required for the desorption of CO. The stabilization of CH$_2$ and CH$_3$ as products at cluster edges makes C−O bond scission in methoxide, hydroxymethyl, and formaldehyde more favorable than on regular (111) facets. Edge-induced stabilization effects were calculated at 23 kJ mol^{-1} for CH$_3$ and at 37 kJ mol^{-1} for CH$_2$. This brings the energy of C−O scission in CH$_2$OH and CH$_2$O close to the thermoneutral threshold and increases the exothermicity of the decomposition of CH$_3$O to CH$_3$ and O.

In Table 1, we also present the dehydrogenation energies of methanol and its derivatives, that is, the energies of hydrogen abstraction from C in CH$_3$OH, CH$_3$O, CH$_2$O, and CHO as well as from O in CH$_2$OH (to produce CH$_2$O) and in CH$_3$OH (to

form CH$_3$O). Here, we used the energy of an H atom at the central fcc site of (111) facets of Pd$_{79}$ as reference. For all intermediates scrutinized, in line with experimental observations,[4–6,8] dehydrogenation is thermodynamically clearly more favorable than C–O bond scission: H abstraction is always exothermic. Slab model data for the dehydrogenation pathway on Pd(111) are very similar.[22]

4.4. Transition States and Activation Barriers for C–O Bond Scission. The transition state (TS) structures of C–O bond scission in methanol, the intermediates CH$_x$O and CH$_2$OH, as well as CO are sketched in Figure 5. Selected interatomic distances are collected in Table 2 (for more details see Supporting Information). The corresponding activation barriers are given in Table 1.

In CH$_3$OH, CH$_3$O, CHO, and CO, bond breaking occurs at C–O distances of 190–200 pm. Similar C–O distances have been calculated for the TS of C–O bond scission on Pd(111): 197 pm for CH$_3$OH,[42] 201 pm for CH$_3$O,[20] and 201 pm for CO.[60] To the best of our knowledge, C–O bond scission of other intermediates of methanol dehydrogenation—CH$_2$OH, CH$_2$O, and CHO—has previously not been studied computationally on Pd surfaces. For hydroxymethyl and formaldehyde, both of which produce CH$_2$ species, we estimated the C–O distance in the TS at ~250 pm, that is, these species exhibit late transition states. However, for the reactants studied, the height of the activation barriers does not seem to correlate with the C–O distance of the TS. Note that the potential energy surfaces of all intermediates are rather flat in the vicinity of the TS. For instance, elongating the C–O distance in CH$_2$O from 200 to 250 pm increases the energy by only 35 kJ mol^{-1}.

The calculated activation barriers obviously depend on the order of the C–O bond to be broken: the lowest barriers, ~130 kJ mol^{-1}, were calculated for the saturated species CH$_3$O and CH$_2$OH with a single, σ-type C–O bond. The barrier in methanol was calculated higher, 158 kJ mol^{-1}, which may be rationalized by the extra energy required to bring *both* centers, C and O, in close contact with the surface in the TS, whereas for CH$_3$O or CH$_2$OH one center (O or C, respectively) is rather strongly bound to the surface already in the initial state. The species CH$_2$O and CHO, where π-contributions strengthen the C–O bond, feature notably higher activation barriers, ~200 kJ mol^{-1}. Interestingly, these two barriers are very similar although the species CH$_2$O and CHO bind to the surface via different mechanisms, which result in very different adsorption energies: 48 kJ mol^{-1} for CH$_2$O, 230 kJ mol^{-1} for CHO. Not unexpectedly, the highest barrier on the Pd cluster, more than 400 kJ mol^{-1}, was calculated for CO dissociation because two bonding π-orbitals strengthen the bond of this molecule.

As discussed in Subsection 4.1, all intermediates considered reveal some activation of the C–O bond as a result of the interaction with the metal surface. This activation can be monitored by the elongation of the C–O bond compared to the corresponding gas phase value. By this criterion, surface-induced bond activation never appears to be strong enough to change the order of the C–O bond. Our results also suggest that the orientation of the C–O bond in the intermediates on Pd (with respect to the surface) plays only a subordinate role in the mechanism of breaking the C–O bond in methanol and its derivatives as adsorbates.[5]

Our data characterize the dissociation of CO on Pd nanoparticles as strongly unfavorable, both for thermodynamic and
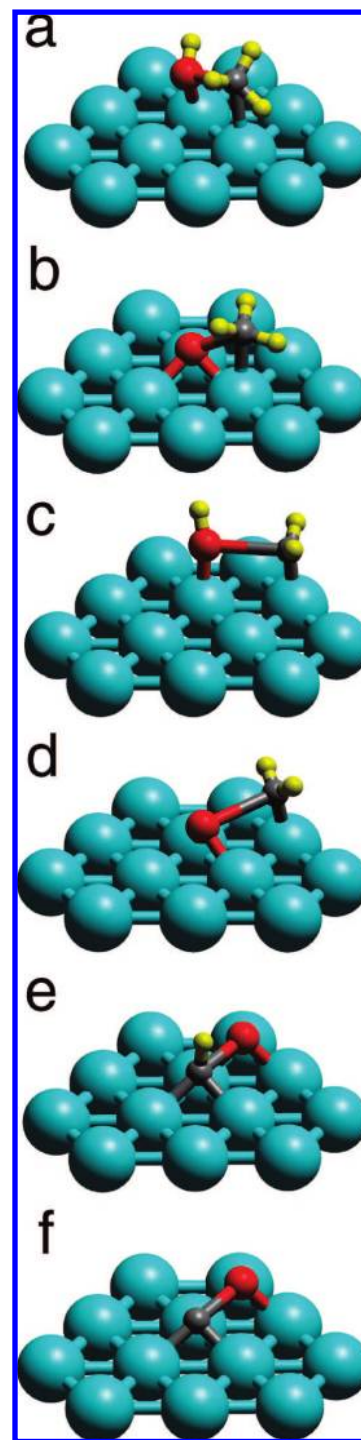
(60) Liu, Z.-P.; Hu, P. *J. Chem. Phys.* **2001**, *114*, 8244.

Figure 5. Transition states of C–O bond scission on a (111) facet of the nanocrystallite Pd$_{79}$: (a) methanol CH$_3$OH, (b) methoxide CH$_3$O, (c) hydroxymethyl CH$_2$OH, (d) formaldexyde CH$_2$O, (e) formyl CHO, and (f) carbon monoxide CO.

kinetic reasons. The reaction is endothermic by 241 kJ mol^{-1} (i.e., it requires more energy than the desorption of the reactant) and the activation barrier is 414 kJ mol^{-1} (Table 1). Thermodynamics and kinetics of CO dissociation are only slightly affected when the reaction proceeds near or at cluster edges of a Pd$_{79}$ nanoparticle. In that case, the activation barrier of a reaction across the edges decreases by 24 kJ mol^{-1} (Figure 6c) and the endothermicity decreases by 21 kJ mol^{-1} due to stronger adsorption of C and O products at 3-fold hollow sites on
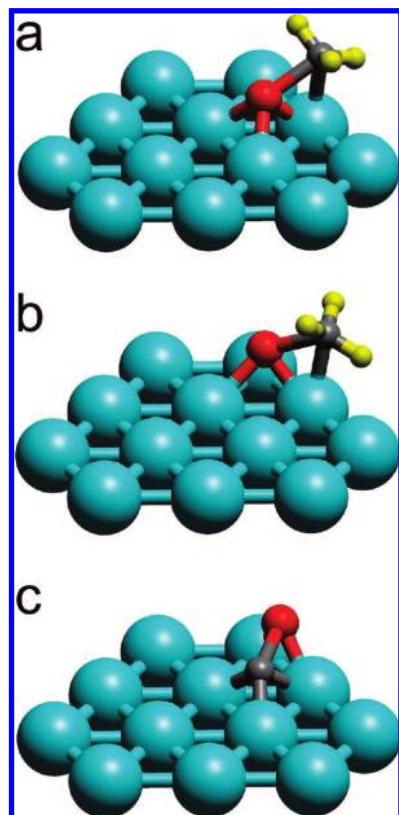
Figure 6. Transition states of C−O bond scission in methoxide CH₃O (a, b) and carbon monoxide CO (c) at an edge where two (111) facets of the nanocrystallite Pd₇₉ meet. In (a) and (b), which differ by positions of the atom O and CH₃O in the initial adsorption complex, methyl group binds to a Pd center at the edge; in (c) the O center of CO is on the way to moving across the edge to the neighboring (111) facet.

different facets near an edge. These results agree with the experimental findings that CO molecules do not dissociate on Pd catalysts.[5,7]

C−O bond breaking in formaldehyde or formyl is also unlikely due to too high activation barriers. Thus, C−O bond breaking in CH₃O and CH₂OH exhibits lower activation barriers than those calculated for other intermediates of methanol dehydrogenation as well as for methanol itself. (In a slab model study of C−O scission of methanol on Pd(111) using the PW91 *xc* functional,[48] the activation barrier was determined at 172 kJ mol⁻¹ and the reaction energy at 14 kJ mol⁻¹; recall the corresponding results calculated in the present study at 158 and 15 kJ mol⁻¹, respectively.)

The activation barriers for C−O bond scission in methoxide and hydroxymethyl, ∼130 kJ mol⁻¹, are still too high for the reaction to compete with the dehydrogenation pathway, which according to slab model calculations features a barrier of 33 kJ mol⁻¹ for C−H bond breaking of CH₃O on the Pd(111) surface.[20,22] Nevertheless, methoxide and hydroxymethyl most probably are the intermediates involved in the very slow C−O bond scission that has been experimentally detected during methanol dehydrogenation on Pd catalysts:[9–11] the decomposition of CH₃O and CH₂OH leads to an accumulation of CH$_x$ deposits on catalyst particles. In fact, we examined here a somewhat idealized mechanism in the sense that we considered pure Pd particles and a low concentration of the reactant. Interaction with impurities (in particular, with CH$_x$ residuals) and/or adsorbate−adsorbate interactions may reduce the activation barriers for C−O bonds scission. Nevertheless, compared

to data just discussed, we do not expect any qualitative change in the interaction parameters of C−O bonds of different intermediates on such modified Pd catalyst.
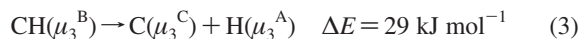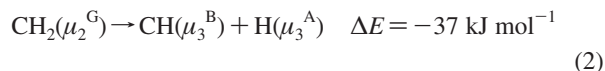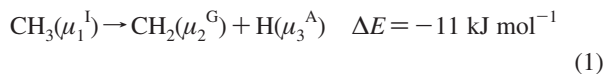
Thus, CH$_x$ decomposition products are expected to first appear at a Pd surface as CH₃ and/or CH₂ fragments. They are rather mobile (see Subsection 4.2), but thermodynamics seems to favor their stabilization at cluster edges. Invoking the Brønsted-Polanyi correlation between reaction energy and activation barrier, one also expects that activation energies of transition states near clusters edges are lower than at the regular Pd(111) surface; this would imply a higher reaction probability at or near edges. The transition states for C−O bond scission in CH₂OH and CH₂O presented above (Figures 5c, d) already involve binding of a CH₂ group to a Pd atom at an edge, and therefore partly account for the stabilizing edge effect. As transition state TS 5b, calculated at first for the splitting of methoxide (Figure 5b), is located inside the (111) facet, we also determined two TS configurations for this species which involve edges, TS 6a and TS 6b (Figures 6a, b). When one considers total energies, TS 6a is almost isoenergetic with TS 5b (in fact, 5 kJ mol⁻¹ higher); in contrast, TS 6b lies 22 kJ mol⁻¹ below TS 5b. However, when one accounts for the stabilization, 29 kJ mol⁻¹, of methoxide in the initial state at a μ_3^K position near an edge (Figure 4a), the activation barrier associated with TS 6b, 144 kJ mol⁻¹, becomes even slightly higher than the barrier of TS 5b in the interior of a (111) facet. The same barrier height is calculated for TS 6b with respect to the initial state with CH₃O initially at a μ_3^B position. Indeed, possible TS configurations near/at nanocluster edges are not limited to the above two cases; further demanding computations might reveal pathways with somewhat lower activation barriers.

However, the activating effect of the edges between two (111) facets is evidently rather moderate, as also indicated by thermodynamics. In this regard, particle edges appear to behave quite differently from steps such as those at Pd(211), where a dramatic stabilization of the TS of CO dissociation was reported.[61] In this context, note that the calculated activation barrier of CO dissociation is only ∼5% lower for the TS, where C−O scission occurs across a cluster edge (Figure 6c), than for the TS within a (111) facet (Figure 5e). Although no strong preference for C−O bond scission at the edges is found, thermodynamics favors the accumulation of CH₃ and CH₂ species at the edges due to diffusion from the facets to the more stable edge positions. CH₃ and CO exhibit very similar binding energies at the edge sites, 180−185 kJ mol⁻¹. [According to our previous study, CO molecules adsorb at nanocluster edges ∼10 kJ mol⁻¹ stronger than at (111) facets,[13] i.e. the stabilizing effect of edges on CO adsorption is slightly smaller than on CH₃ adsorption.] Thus, CH₃ and CO species are expected to compete for adsorption at edges, although CH₃ adsorbs on top while CO prefers bridge sites. In turn, CH₂ species with adsorption energy of ∼400 kJ mol⁻¹ (Table 3) are definitely able to block bridge-at-edge positions for CO adsorption.

There is experimental evidence[5] that carbonaceous species, preventing CO adsorption, block predominantly hollow sites near cluster edges, indicating the presence of C and CH rather than CH₂ and CH₃ species. One can resolve this apparent contradiction by invoking fast dehydrogenation of CH₂ and CH₃ species adsorbed at cluster edges to CH and C, which will then occupy hollow sites near edges and exhibit a much lower mobility on the surface of a nanoparticle. Indeed, full dehy-

(61) Liu, Z.-P.; Hu, P. *J. Am. Chem. Soc.* **2003**, *125*, 1958.

drogenation of CH$_3$ to C at or near edges of a Pd$_{79}$ particle is exothermic. For various adsorption sites (given in parentheses, see Figure 4) we obtained:

$$CH_3(\mu_1^I) \rightarrow CH_2(\mu_2^G) + H(\mu_3^A) \quad \Delta E = -11 \text{ kJ mol}^{-1} \tag{1}$$

$$CH_2(\mu_2^G) \rightarrow CH(\mu_3^B) + H(\mu_3^A) \quad \Delta E = -37 \text{ kJ mol}^{-1} \tag{2}$$

$$CH(\mu_3^B) \rightarrow C(\mu_3^C) + H(\mu_3^A) \quad \Delta E = 29 \text{ kJ mol}^{-1} \tag{3}$$

Thus, transformation of CH$_3$ and CH$_2$ to CH is energetically favorable and the final step, leading to "bare" C centers, is moderately endothermic (Figure 1). A recent DF slab model study of methane dehydrogenation on Pd(001) furnished activation barriers of $30-70$ kJ mol^{-1} for various reaction steps.[62] Thus, when compared to the activation barrier of 130 kJ mol^{-1} calculated in this work for C$-$O bond scission, one concludes that dehydrogenation of CH$_3$ or CH$_2$ species on Pd is much faster than the formation of these species via methoxide or hydroxymethyl decomposition. Therefore, there is no contradiction between C$-$O bond scission in methoxide or hydroxymethyl according to our computational results and the experimentally observed accumulation dehydrogenated species C or CH.[5]

5. Summary and Conclusions

We studied the reaction path for C$-$O bond scission in various intermediates of methanol decomposition at the surface of Pd nanoparticles by DF calculations. Our goal was to reveal the mechanism how Pd catalysts become modified by carbon and carbonaceous species, which according to experiment[4–7] are formed at low rates as byproducts of methanol dehydrogenation. Pursuing our recently proposed modeling approach, a Pd$_{79}$ nanocrystallite of cuboctahedral shape was used to represent model catalysts built of well-ordered supported Pd particles containing $\sim 10^3$ atoms. Compared with previous applications of this modeling strategy, the overall symmetry of the nanoclusters models was reduced far enough to study comprehensively the adsorption of intermediates as well as transition states for C$-$O bond scission of CH$_3$OH, CH$_3$O, CH$_2$OH, CH$_2$O, CHO, and CO—*without any local* geometry restriction of the surface complexes.

The energies of C$-$O bond scission, calculated for a variety of intermediates of methanol decomposition, and the corresponding activation barriers show that C$-$O bond scission is likely to proceed as a very slow by-process that accompanies the dehydrogenation pathway (Figure 1), most probably in the intermediates with a single (σ-type) C$-$O bond, that is, CH$_3$O and CH$_2$OH. Compared to the latter species, CH$_2$O and CHO, intermediates with a π-contribution to the C$-$O bond, exhibit much higher activation barriers for C$-$O scission. The highest activation barrier of C$-$O bond breaking was calculated for the final product of methanol dehydrogenation, CO, the species where this bond is strongest due to a notable π-contribution. Moreover, dissociation of CO on Pd nanoparticle is strongly endothermic.

We addressed in detail the role of low-coordinated (edge) sites on Pd nanoparticles in accelerating the catalyst contamination by decomposition of CH$_x$ species. In particular, CH$_3$ and CH$_2$ products of CH$_3$O and CH$_2$OH decomposition were found to occupy preferentially positions at the edges of the Pd$_{79}$ nanoparticle. Computational results suggest that CH$_3$ and CH$_2$ species undergo fast dehydrogenation to CH and C.

The present theoretical study quantified in detail the mechanism of catalyst modification in a process of general importance. This was achieved with the help of the first large-scale application of our novel efficient modeling scheme for problems of surface reactivity, where nanocrystallites are used to describe complex substrates.

Supporting Information Available: Cartesian coordinates of pertinent structures and full version of ref 25. This material is available free of charge via the Internet at http://pubs.acs.org.

(62) Zhang, C. J.; Hu, P. *J. Chem. Phys.* **2002**, *116*, 322.

JA078322R